Journal of Hazardous Materials 340 (2017) 435–444

Contents lists available at ScienceDirect

Journal of Hazardous Materials

journal homepage: www.elsevier.com/locate/jhazmat

Natural magnetic pyrrhotite as a high-Efficient persulfate activator for micropollutants degradation: Radicals identification and toxicity evaluation

Dehua Xia[a,b,1], Ran Yin[c,1], Jianliang Sun[c], Taicheng An[d,*], Guiying Li[d], Wanjun Wang[d], Huijun Zhao[e,f], Po Keung Wong[a,*]

[a] School of Life Sciences, The Chinese University of Hong Kong, Shatin, NT, Hong Kong SAR, China
[b] School of Environmental Science and Engineering, Sun Yat-sen University, Guangzhou, 510275, China
[c] Department of Civil and Environmental Engineering, The Hong Kong University of Science and Technology, Clear Water Bay, Kowloon, Hong Kong SAR, China
[d] Institute of Environmental Health and Pollution Control, School of Environmental Science and Engineering, Guangdong University of Technology, Guangzhou, 510006, Guangdong, China
[e] Centre for Clean Environment and Energy, Griffith Scholl of Environment, Griffith University, Queensland 4222, Australia
[f] Laboratory of Nanomaterials and Nanostructures, Institute of Solid State Physics, Chinese Academy of Sciences, Hefei 230031, Anhui, China

HIGHLIGHTS

- The NP can efficiently activate PS and H_2O_2 to degrade phenol.
- Aerobic and acidic conditions favors the generation of $^{\bullet}SO_4^-$ and $^{\bullet}OH$.
- Leached and surface Fe^{2+} of NP collectively work for PS activation.
- Phenol degradation was inhibited but with TOC removal in real water matrixes.
- Acute toxicity test showed a fluctuating trend of phenol treated in surface water.

GRAPHICAL ABSTRACT

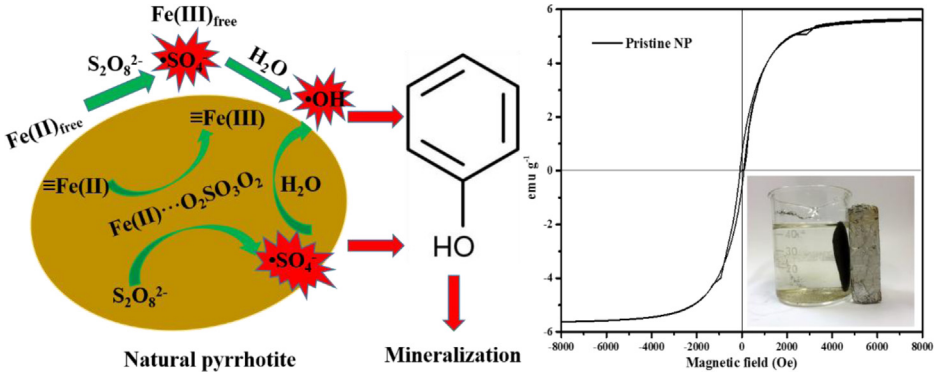

ARTICLE INFO

Article history:
Received 11 April 2017
Received in revised form 27 June 2017
Accepted 12 July 2017
Available online 20 July 2017

Keywords:
Sulfate radical
Persulfate
Natural pyrrhotite

ABSTRACT

This study discusses the $^{\bullet}SO_4^-$ based process mediated by natural magnetic pyrrhotite (NP) for the degradation of refractory organic micropollutants. Complete degradation of 20 μM phenol in distilled water (DW) was obtained within 20 min using NP/PS (persulfate) system. Electron paramagnetic resonance spectra indicated aerobic and acidic conditions favored the generation of both $^{\bullet}SO_4^-$ and $^{\bullet}OH$ species, but only $^{\bullet}OH$ signal was survived at alkaline condition. The leaked Fe^{2+} and ≡Fe(II) of NP collectively work to activate PS and generate surface and bulk $^{\bullet}SO_4^-$ and $^{\bullet}OH$ simultaneously. The identified intermediates indicate the transformation of benzene ring is the key step for phenol degradation by NP/PS system. Moreover, phenol degradation was greatly inhibited in surface water (SW, 29%) and wastewater (WW, 1%), but 25.9% and 17.5% of TOC removal were obtained in the SW and WW during

Abbreviations: NP, Natural pyrrhotite; PS, Sodium persulfate; EPR, Electron paramagnetic resonance; ROS, Reactive oxygen species; AOPs, advanced oxidation processes; TBA, tert-butanol alcohol; TOC, Total organic carbon; SW, Surface water; WW, Wastewater.

* Corresponding authors.
E-mail addresses: antc99@gdut.edu.cn (T. An), pkwong@cuhk.edu.hk (P.K. Wong).
[1] These authors contributed equally to this work.

http://dx.doi.org/10.1016/j.jhazmat.2017.07.029

Phenol degradation
Eco-toxicity

NP/PS treatment, respectively. Additionally, the acute toxicity tests for NP/PS process exhibited a fluctuating trend depending on the water matrix, while the genotoxic activity analysis indicated that the treated phenol solutions were not genotoxic but cytotoxic. Overall, this study provides a solution to abate refractory organic micropollutants in water systems.

1. Introduction

Organic micropollutants, such as pharmaceuticals and personal care products, endocrine disrupting compounds and phenols, widely occur in various aqueous environments, such as surface water and secondary sewage effluents [1–3]. Organic micropollutants pose potential threats to human health as well as aquatic ecosystems [4]. Many micropollutants, including pesticides, solvents and pharmaceuticals, are refectory to the conventional treatment approaches, such as biodegradation, coagulation, sedimentation and chemical oxidation [5,6]. In the past decades, advanced oxidation processes (AOPs) like persulfate and H_2O_2 activation process, which generate powerful oxidative reactive radicals to quickly degrade the recalcitrant organic pollutants in aqueous solution, have become promising alternative technologies [7–9]. Therefore, application of advanced oxidation processes (AOPs) is needed for the removal of the refractory organic micropollutants.

Sulfate radical ($^{\bullet}SO_4^-$)-based AOPs are becoming emerging alternatives to the common hydroxyl radicals ($^{\bullet}OH$)-based AOPs. With a redox potential of 2.5–3.1 V, $^{\bullet}SO_4^-$ has strong oxidizing capability and can degrade different types of recalcitrant organic compounds with a second order rate constant ranging from 10^6 to 10^8 $M^{-1}s^{-1}$ [10]. Generally, the cheap peroxydisulfate (PS; $S_2O_8^{2-}$) is one of the widely-used reagent to produce $^{\bullet}SO_4^-$ [11,12], which can be activated by different methods, such as UV, heat, transition metals and metal-containing oxides [13–15]. Among them, ferrous (Fe(II)) is promising for application, owing to the its environmental-friendly nature and cost-effectiveness [16]. However, the Fe(II)/PS system has several defects, including rapid oxidation of Fe(II), limitations to low pH range and the production of iron sludge [17]. To alleviate these disadvantages, several iron-based activators were developed as alternatives, including zero-valent iron (ZVI) [18], Fe_3O_4 [19], Fe@Fe_2O_3 [20], iron immobilized silica [21], (Co, Cu, and Zn)Fe_2O_4 [22], $CuFeO_2$ [23], and MnO_2/$ZnFe_2O_4$ [24], etc. Most of these synthetic materials exhibit promising activation performance, but the massive production of such materials at low cost is a major limitation to their widespread application.

Recently, several irons ores, such as goethite, ferrihydrite, pyrolusite, have been investigated for the activation of persulfate [25–27]. These minerals are promising for application, due to their earth abundance and easy availability at a low cost in mineral deposit. Very recently, natural pyrrhotite (NP, $Fe_{1-x}S$) mineral also shows promising future for PS activation: its specific ferromagnetic properties could facilitate phase separation, making it more superior than other minerals [28]. Xia et al. have successfully utilized NP to activate PS for *E. coli* inactivation and identified the vital role of sulfate radical [29]. However, many issues are still not well understood of this NP/PS process which deserve further investigation: (1) the generated reactive species may vary with different O_2 or pH conditions; (2) the role of surface and bulk ROS for organic micro-pollutant degradation during NP/PS treatment are unknown; (3) the ecotoxicological risks for the removal of organic micro-pollutants in different water matrix are obscure.

Therefore, to fill the research gaps, the NP/PS process was utilized to degrade refractory organic micropollutants in different water matrix. Phenol, widely occurs in water and soil and can't be effectively removed by the conventional biodegradation or coagulation [30], was selected as a model micro-pollutant. The variations of generated radicals in different water conditions were identified using electron paramagnetic resonation (EPR) analysis and quantified using a competition kinetic model. A radical-induced degradation pathway of phenol was analyzed and proposed. Moreover, acute and genotoxic effects of the initial phenol and its degradation products were studied under optimized treatment conditions to examine the ecotoxicological safety of the proposed treatment systems.

2. Materials and methods

2.1. Chemicals

Phenol, methanol, and *tert*-butanol alcohol (TBA) were obtained from Sigma-Aldrich, USA. Sodium persulfate (PS), Catalase, 5,5-dimethyl-1-pyrrolidine N-oxide (DMPO) were purchased from Aladdin, China. Pristine NP was collected from a mining site in China. The raw mineral was machine crushed, and then selected by an electromagnetic and gravity separator. Before use, the picked NP was sieved at 300-mesh to obtain final powders with size smaller than 38 μm.

2.2. Experimental procedures

In batch trials, the NP particles (0.5–5 g L^{-1}) were added to 50 mL solution containing phenol (20 μmol L^{-1}) in a flask, followed by adding sodium persulfate solution (0.05–1.0 mmol L^{-1}) to initiate the reaction. Aqueous samples (1 mL) were collected by syringes at scheduled time intervals, filtered with 0.22-μm syringe filters (Darmstadt, Germany), and transferred into 2-mL autosampler vials for chromatography analysis. Excess ethanol/catalase (200 μL) was immediately added into the vials to quench persulfate/H_2O_2 and protect phenol from further degradation [31]. To study the pH effect, the reaction was conducted in phosphate-buffered saline (5 mmol L^{-1}) at different pHs. Moreover, samples after filtration were analyzed for remaining phenol, TOC, and PS concentrations.

2.3. Analytical methods

The phenol concentration was determined using a high-performance liquid chromatograph (HPLC, Shimadzu 6A) equipped with a TSK-GEL ODS-100S column and a UV detector set at 270 nm. An isocratic eluent of methanol and water (v/v, 70/30) was used as the mobile phase with a constant flow rate (0.8 mL/min). The intermediates and products of phenol, after the aforementioned pretreatment, were identified with a Waters UPLC system coupled to the Waters Acquit ESI-tqMS device (UPLC/ESI-tqMS) and equipped with a HSS T3 column (50 × 2.1 mm, 1.8 μm particle size, Waters). The mobile phase was composed of methanol and water at a flow rate of 0.4 mL/min with the column temperature of 35 °C. The composition of methanol/water (v/v%) changed linearly from 5:95 to 90:10 in the first 8 min, returned to 10:90 in the next 0.1 min, and then changed linearly back to 5:95 in the following 2.9 min. The accurate *m*/*z* and the proposed chemical

Table 1
Parameters of surface water and secondary wastewater effluent.

Parameter	SW	WW
TOC ($mg\,L^{-1}$)	7.8	10.2
COD ($mg\,O_2\,L^{-1}$)	nd	<30
SS ($mg\,L^{-1}$)	12	14
TN ($mg\,N\,L^{-1}$)	nd	5.3
TP ($mg\,P\,L^{-1}$)	nd	1.2
Alkalinity ($mg\,CaCO_3\,L^{-1}$)	11.5	17.6
Hardness ($mg\,CaCO_3\,L^{-1}$)	110	113
UV_{254} (cm^{-1})	0.043	0.202
pH	8.3	7.64

nd=non-detected.

formula were obtained from a Bruker maxis 4G UPLC/ESI-QTOF-MS system equipped with an Agilent SB-C18 column (50 × 2.1 mm, 1.8 μm particle size). The mobile phase consisted of water and acetonitrile (ACN) at a flow rate of 0.4 mL/min. The composition of ACN/water (v/v%) changed linearly from 5:95 to 90:10 in the first 8 min, remained at 90:10 for 10 min and returned to 10:90 in the next 0.1 min, then changed linearly back to 5:95 in the following 2.9 min [32]. The leaked metal ions were quantified by inductively coupled plasma-optical emission spectrometer (ICP-OES, ULTIMA 2000, HORIDA). An Electron Paramagnetic Resonance (EPR) Spectrometer Bruker A300 was used to identify the radicals, and was set up as follows: microwave frequency at 9.8752 GHz, sweep width at 100 G, center field at 3504.12 G, modulation amplitude at 1 G, time constant at 327.68 ms, and scan time of 40 s. Before EPR test, 1-ml of 0.5 mol L^{-1} DMPO was added to 50 mL of the reaction mixture to react for 20 min [33].

2.4. Water and wastewater samples

The surface water sample (SW) was taken from the influent of the Waiyuan lake in the Chinese university of HongKong, whereas the wastewater sample (WW) was obtained from the outlet of Shatin municipal wastewater treatment plant practicing advanced biological treatment. The environmental characteristics of SW and WW samples were provided in Table 1. The TOC of the samples was measured on a Shimadzu VPCN analyzer (Japan). Residual PS concentrations were traced by employing colorimetric methods according to Villegas et al. [34]. The UV absorbance of the water/wastewater samples was measured on a Perkin Elmer Lambda 25 spectrophotometer in 1-cm quartz cuvettes. Anion analysis was conducted using a Dionex ICS-1500 ion chromatograph unit equipped with a conductivity detector, a Dionex IonPac AG14A (4 × 50 mm) guard column and a Dionex IonPac AS14A (4 × 250 mm) analytical column.

2.5. Acute toxicity and genotoxicity

The acute toxicity towards the photobacterium V. fischeri was measured during NP/PS treatment of phenol in DW and SW using a commercial bioassay kit (BioToxTM, Aboatox Oy, Finland) according to the ISO 11348-3 test protocol. After mixing 500 μL of the initial or treated phenol solutions with 500 μL luminescent bacterial suspensions, the light emission after 15 min contact time was measured at a temperature of 15 °C. Percent relative inhibition rates were calculated on the basis of a toxicant-free control [35].

The detection of genotoxicity was conducted with UMU-ISO 13829 test kit. The genotoxic effects of the initial and treated samples were determined by calculating the growth factor G, b-galactosidase activity *Us* and induction ratio I_R for each sample dilution relative to the respective blank and negative/positive controls in accordance with the test protocol. Several dilutions (1:1.5, 3.0, 6.0 and 12.0) of the original phenol solution and treated samples in DW were prepared for the test. The obtained results were accepted as valid if G > 0.5 and the positive controls reach an I_R value > 2. A test sample is considered to be genotoxic if its I_R value is >1.5 [36].

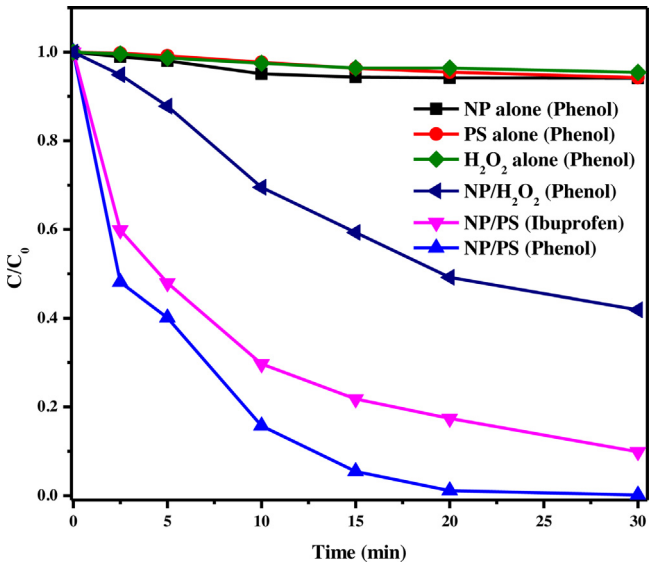

Fig. 1. Degradation profiles of phenol/ibuprofen by NP activated persulfate and H_2O_2 system. Experimental conditions: [phenol or ibuprofen] = 20 μmol L^{-1}, [PS] = [H_2O_2] = 0.5 mmol L^{-1}, [NP] = 1.25 g L^{-1}.

3. Results and discussions

3.1. Reactivity of NP/PS process

Natural occurring pyrrhotite (NP) was identified as monocline pyrrhotite ($Fe_{1-x}S$, PDF 29-0725) with a saturation magnetization of approximately 6 emu g^{-1} with little coercivity (12 Oe) and remanence (0.06 emu g^{-1}) (Fig. S1). NP contained many Fe^{2+} would be able to trigger Fenton-like processes to a significant extent, thus catalytic activity of persulfate ($S_2O_8^{2-}$) by NP was also compared with hydrogen peroxide (H_2O_2) activation. As shown in Fig. 1, PS or H_2O_2 alone is not being capable of degrading phenol, and the adsorption of phenol by NP was weak (NP only). Actually, the electrostatic effect is an important factor that can affect the interaction between pollutant and catalyst. As shown in Fig. S2, the zeta potential of NP was determined to be 4.6. Meanwhile, the pKa value of phenol is 9.99, hence below this pH phenol is considered a neutral molecule and above this value it is in the anionic form [37,38]. Actually, the pH after reaction was decreased to an equivalent value of 5.4 (Fig. S3). This result of pH change was discussed in the section 3.4. At the tested pH values (5.4) in this study, no matter NP surface was positively (e.g., at pH 3) or negatively (e.g., at pH 7 and 9) charged, phenol was all in neutral form in solution. Therefore, there is no significant attraction or repulsion between phenol and NP, from the electrostatic point of view. Obviously, the NP could effectively activate PS to degrade phenol and almost 100% of the phenol (2 μmol L^{-1}) was degraded within 20 min. In contrast, only 59% phenol degradation was observed after 30 min upon activation of H_2O_2 with NP. These results indicate the NP is active for both PS and H_2O_2 activation. Moreover, the selectivity of $^{\bullet}SO_4^-$ for reaction with organic compounds may also cause the tendency of phenol degradation in persulfate systems was more than that of $^{\bullet}OH$ in H_2O_2, particularly when the reaction pH is acidic [39]. In order to further check the ability of the NP/PS oxidation system in degrading other refractory organic pollutants, the degradation assay towards ibuprofen was carried out, a typical pharmaceu-

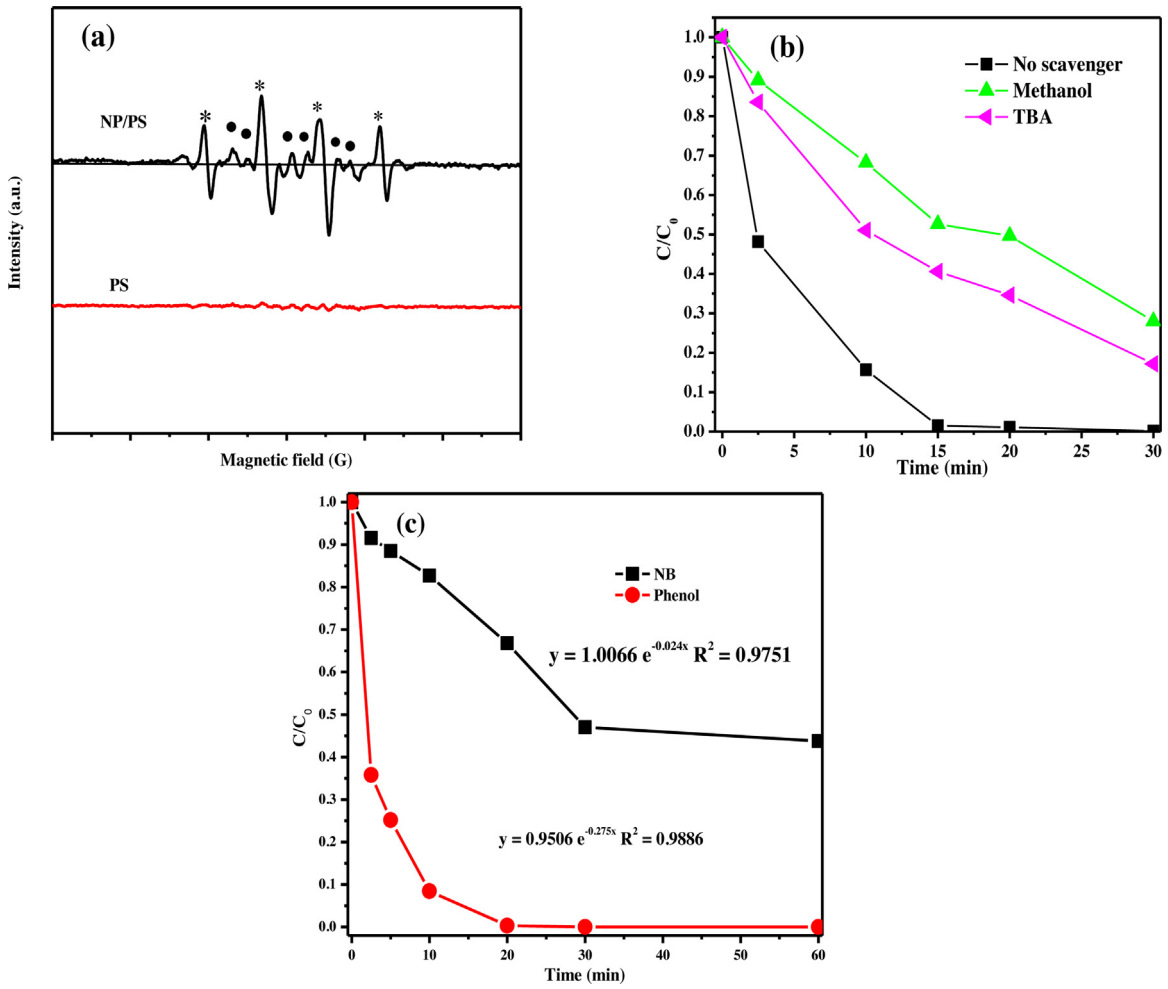

Fig. 2. (a) EPR signals of radical generation in NP/PS system (DMPO-•OH; DMPO-•SO_4^{2-}); (b) Inhibition effect of *tert*-butyl alcohol (TBA), methanol on phenol degradation by NP/PS system; (c) Degradation of nitrobenzene (NB) and phenol in NP/PS system. Experimental conditions: [phenol] = 20 μmol L^{-1}, [PS] = 0.5 mmol L^{-1}, [NP] = 1.25 g L^{-1}, [methanol] = [TBA] = 5 mmol L^{-1}, [NB] = 10 μmol L^{-1}.

tical pollutant. More than 90% of the initial ibuprofen could be degraded within 30 min, illustrating the NP/PS system also efficient towards degrading ibuprofen. This indicates the degradation mechanism of NP/PS system was pollutant independent. Moreover, phenol degradation efficiency depends heavily on the increased amount of added NP and dosage of PS (Fig. S4), and the optimal concentration of NP and PS is 1.25 g L^{-1} and 0.25 mmol L^{-1}, respectively. When higher dosage of NP (5 g/L) was utilized, the excessive Fe^{2+} in NP will consume/scavenge the formed radicals (•SO_4^-/•OH) and thus cause lower phenol removal, as Fe^{2+} has a large rate constant (~10^7 $Lmol^{-1}s^{-1}$) towards •SO_4^-. Similar results were also obtained in other reference [28].

3.2. Identification of reactive species

Radical process was well recognized in terms of the *E. coli* inactivation mechanism involved in the NP activated PS system [27]. Similarly, the EPR experiments were performed to detect radicals generated in the NP/PS system and the results are shown in Fig. 2a. Without air purging and pH adjustment, six-line spectrum with relative intensities of 1:1:1:1:1:1 and four characteristic peaks with a 1:2:2:1 quarter pattern were observed simultaneously, suggesting the generation of •SO_4^- and •OH in the system [40]. To verify the relative contributions of •SO_4^- and •OH to phenol degradation in the NP/PS system without air purging and pH adjustment, quenching tests were carried out using methanol and TBA. Methanol with an α hydrogen ensures the quenching of both •SO_4^- (second-order rate constant 1.1×10^7 $Lmol^{-1}s^{-1}$) and •OH (second-order rate constant 9.1×10^8 $Lmol^{-1}$ s^{-1}) owing to the high reactivity toward the two radicals, whereas TBA without an α hydrogen mainly reacts with •OH (6×10^8 $Lmol^{-1}$ s^{-1}) and is not effective for •SO_4^- (4×10^5 $Lmol^{-1}$ s^{-1}) [29].

In the presence of methanol, the phenol degradation efficiency after 30 min reaction time was decreased to 83% (Fig. 2b). In contrast, the phenol degradation efficiency was decreased to 72% with TBA added. Since TBA is relatively reactive with •OH but almost inert towards •SO_4^-, the slight lower scavenging effect (11%) than methanol probably suggests that •OH and •SO_4^- both contributed to the phenol degradation.

To further differentiate the relative contributions of •SO_4^- and •OH, the concentrations of •SO_4^- and •OH at steady-state ($[•SO_4^-]_{ss}$, $[•OH]_{ss}$) were quantified using specific probes during phenol degradation (Fig. 2c). Nitrobenzene (NB) was selected as the indicator of •OH for its large rate constant towards •OH (3.9×10^9 $Lmol^{-1}s^{-1}$) and a much smaller rate constant towards •SO_4^- ($\leq 10^6$ $Lmol^{-1}s^{-1}$) [20]. NB exhibited poor degradation by PS or NP alone (Fig. S5), but degraded considerably in the NP/PS system, thereby further confirming the formation of •OH in NP/PS system. Since both •OH and •SO_4^- were participated into phenol degradation, thereby the kinetic expressions of phenol and

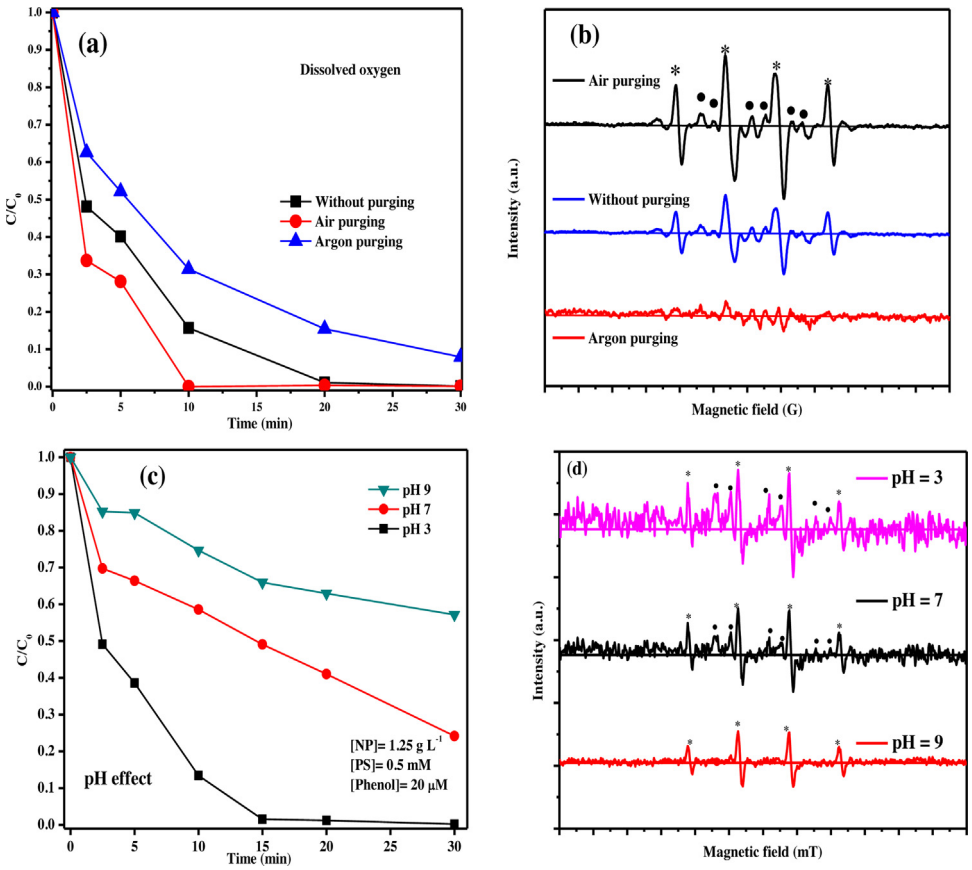

Fig. 3. Influences of (a) dissolved oxygen and (c) initial pH for phenol degradation in NP/PS system; (b) effect of oxygen and (d) pH on radical generation in NP/PS system. Experimental conditions: [phenol] = 20 μmol L^{-1}, [PS] = 0.5 mmol L^{-1}, [NP] = 1.25 g L^{-1}.

nitrobenzene degradation by NP/PS system could be expressed by the following Eqs. (1)–(2).

$$\frac{-dC_{NB}}{dt} = K_1\,[\cdot OH]\cdot C_{NB} = K_{O,NB}\cdot C_{NB} \quad (1)$$

$$\frac{-dC_{phenol}}{dt} = K_2\,[\cdot OH]\cdot C_{phenol} + K_3\,[\cdot SO_4^-]\cdot C_{phenol} = K_{O,phenol}\cdot C_{phenol} \quad (2)$$

In this expression, k_1 is the rate constant between •OH and nitrobenzene (k_1 = 3.2-4.7 × 10^9 $Lmol^{-1}$ s^{-1}), k_2 is the rate constant between •OH and phenol (k_2 = 6.6 × 10^9 $Lmol^{-1}$ s^{-1}), and k_3 is the rate constant between $•SO_4^-$ and phenol (k_3 = 8.8 × 10^9 $Lmol^{-1}$ s^{-1}) [40]. $k_{0,NB}$ ($k_{o,NB}$ = 0.024 mol^{-1} s^{-1}) and $k_{0,phenol}$ ($k_{o,phenol}$ = 0.275 mol^{-1} s^{-1}) are the observed rate constants of nitrobenzene and phenol degradation [40]. C_{NB} and C_{phenol} are the initial concentrations of nitrobenzene and phenol.

$$\frac{K_{o,phenol}}{K_{o,NB}} = \frac{0.275}{0.024} = 11.5 > \frac{K_2}{K_1} = 1.4\sim2.1 \quad (3)$$

The value of $k_{0,phenol}/k_{0,NB}$, obtained from log fit of phenol and nitrobenzene degradation was 11.5 (Eq. (3)). It was much larger than the value of k_2/k_1 (1.4 ~ 2.1), indicating the primary contribution of $•SO_4^-$ rather than •OH to phenol degradation. Moreover, the estimated concentrations of $[•SO_4^-]_{ss}$ (7.85 × 10^{-13} mol L^{-1}) was 4.31 times higher than that of $[•OH]_{ss}$ (1.82 × 10^{-13} mol L^{-1}). Therefore, the present study indicates the rank of ROS for phenol degradation is $•SO_4^-$ > •OH.

3.3. Effect of oxygen and pH

Effects of oxygen content on the radicals' generation were investigated in the NP/PS system. Obviously, the phenol removal rate was 100% after 10 min with air purging and after 20 min without air purging, while 80% under argon purging after 30 min reaction (Fig. 3a). Interestingly, on the EPR pattern, both characteristic peaks with a higher intensity were obtained after air purging than argon purging, indicating more generation of both reactive species (Fig. 3b). This is consistent with previous report that the increase of O_2 concentration could accelerate the radical chain reactions through molecular oxygen activation [41].

In addition, two experiments at pH 3, 9 were conducted to analyze the effects of solution pH on the radicals' generation in the NP/PS system. As shown in Fig. 3c, the elimination of phenol was 100% at pH 3.0 and 44.1% at pH 9.0 within 30 min, respectively. Interestingly, both $•SO_4^-$ and •OH with higher peaks were clearly identified under pH 3.0 condition, while only •OH signal was mainly observed in the pH 9.0 system (Fig. 3d). Under acidic pH conditions, NP could release more Fe^{2+} to activate PS [42]. In alkaline condition, the inhibited performance was mainly led by the precipitation of Fe^{3+} ions to form oxyhydroxides like $FeOH^{2+}$/$Fe(OH)_{2+}$ [43], which have low efficiency for activating PS to form $•SO_4^-$. Moreover, it has been reported that •OH can form in alkaline solution due to the base activation of PS [43]. Therefore, both aerobic and acidic conditions are beneficial for phenol degradation in NP/PS system.

3.4. Role of surface and bulk radical

The Fe ions leaching in the NP/PS system were monitored, because free Fe ions can efficiently activate PS to produce $•SO_4^-$.

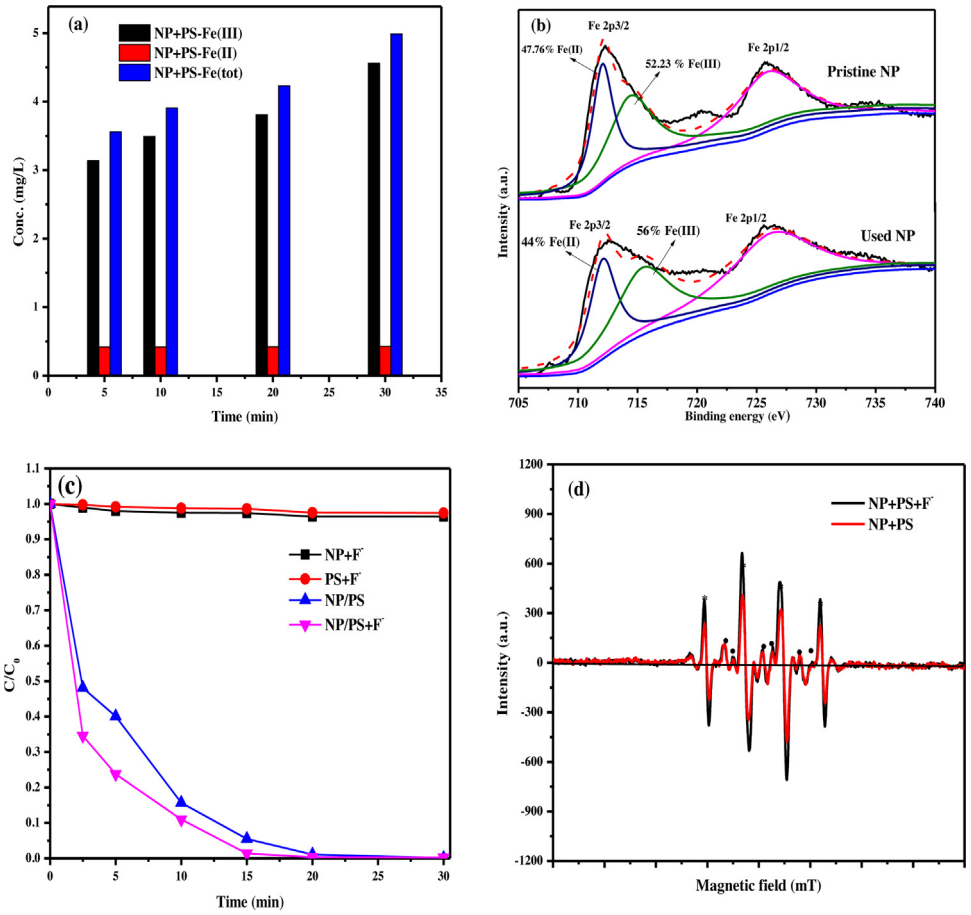

Fig. 4. (a) Leakage of Fe^{2+} and Fe^{3+} in NP/PS system; (b) XPS of Fe spectra in pristine NP and used NP; (c) phenol degradation and (d) EPR spectra in NP/PS and NP/PS/F^- system. Experimental conditions: [phenol] = 20 μmol L^{-1}, [F^-] = 5 mmol L^{-1}, [PS] = 0.5 mmol L^{-1}, [NP] = 1.25 g L^{-1}.

As shown in Fig. 4a, the concentration of total leaching Fe ions is at a level of 0.089 mmol L^{-1} after 30 min reaction, in which Fe^{2+} ions kept below 0.007 mmol L^{-1} while Fe^{3+} ions sharply increased to a concentration of 0.078 mmol L^{-1} in the initial 5 min and then slowly increased to a concentration of 0.082 mmol L^{-1}. This suggests that NP could release Fe^{2+} ions dynamically, and then reacted with PS instantly to form into Fe^{3+} ions and $^{\bullet}SO_4^-$/$^{\bullet}OH$ in bulk. Other works also mentioned the superficial corrosion of pyrite (FeS) [38,39], similar component to pyrrhotite ($Fe_{1-x}S$).

As a Fe^{2+} source, the surface ≡Fe(II) of NP may also trigger the heterogeneous activation rather than free Fe ions. The high resolution XPS spectra for Fe 2p regions of fresh and used NP were also recorded and given in Fig. 4b. Clearly, after activation, the proportion of Fe (II) species declined from 47.76% to 44%, indicating the oxidation of Fe (II) into Fe (III) species on the surface of NP. Moreover, ATR-FTIR spectrum indicates that a small specific peak at 1009 cm^{-1} in NP suspension blue-shifted to 1024 cm^{-1} in NP/PS system, confirming the interaction and formation of a weak complex on the NP surface (Fig. S6). Therefore, phenol degradation was attributed to both homogeneous reactions with leached Fe^{2+} ions and heterogeneous reaction with ≡Fe(II) to activate PS.

To further analyze the role of surface bound $^{\bullet}OH$/$^{\bullet}SO_4^-$ generated by the surface bound Fe(II) on NP, an F^- surface modification was used to remove the surface radicals because F^- shows strong and stable adsorption on catalyst and desorbs surface radicals on the catalyst by adopting fluoride-exchange [44]. It should be noted that, after F^- surface modification, the decrease of surface radicals may promote the production of radicals in bulk. As expected, the phenol degradation is considerably enhanced with 1 mM of F^- modification, indicating the surface radicals is important rather than the radicals in bulk for phenol degradation (Fig. 4c). Moreover, the addition of F^- improved the intensity of DMPO trapped $^{\bullet}OH$/$^{\bullet}SO_4^-$ ESR signal by 10% in the NP/PS system after 120-s of reaction, well validating that the surface-bound ROS was generated by the surface bound Fe(II) on NP in the NP/PS system (Fig. 4d).

3.5. Identification of intermediates and transformation pathways

The intermediates/products of radical-induced degradation of phenol were also investigated by using UPLC/ESI-tqMS. As shown in Fig. 5a, b, acetic acid (*m/z* 59.26), phenoxy radicals (*m/z* 93.20), benzoquinone (*m/z* 109.15), salicylic acid (*m/z* 137.11) and some polymeric compounds were found to be the major intermediates/products. Based on these intermediates/products identified, a pathway of phenol degradation by the NP/PS process is proposed in Fig. 5c. The generated $^{\bullet}SO_4^-$ and $^{\bullet}OH$ first oxidized phenol to phenoxy radicals and form benzoquinone. Meanwhile, the phenoxy radicals may recombine or condensate with phenol molecules to form polymeric compounds [45]. Moreover, the radicals might further attack the aromatic ring of benzoquinone, the phenolic derivatives then transformed into smaller molecular acids via a series of ring-opening, H abstraction, and addition reactions. This pathway was consistent with that observed by Li et al. [46]. Moreover,

Fig. S3 shows that the pH decreased in the initial during NP/PS treating phenol, mainly attributed to the formation of acidic decomposition products, further degraded causing stable pH at the later stage of the reaction. However, in the case of NP/H_2O_2, phenol

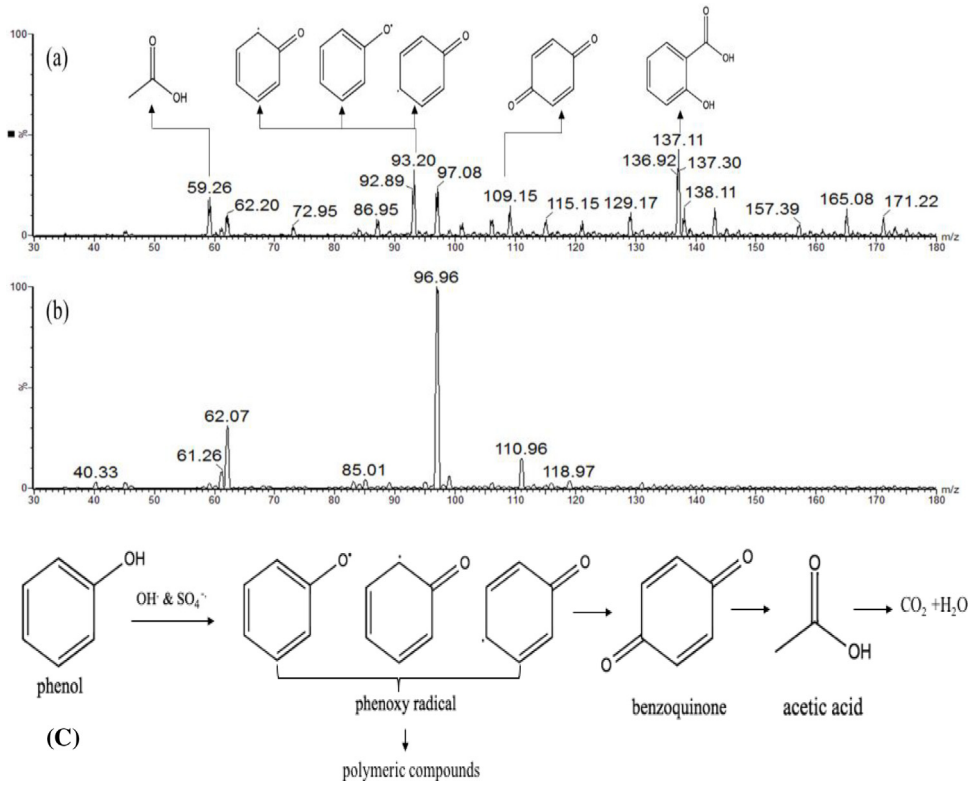

Fig. 5. (a) Mass spectrum of intermediates from phenol degradation; (b) Mass spectrum of blank; and (c) Proposed radical-induced degradation pathway of phenol by NP/PS process.

was degraded to acidic decomposition products initially but with an increase in the reaction time, for the reason that these acidic degradation products were further degraded and neutralized by steps of formation of OH^- causing little elevation of pH.

3.6. Degradation of phenol in authentic water

In order to elucidate the effect of different water and wastewater matrices on phenol removal with the NP/PS system, the DW, SW and WW samples spiked with 20 μmol L^{-1} of phenol were subjected to this treatment process. Notably, the addition of phenol (TOC = 0.72 mg C L^{-1}) was not the main contributor to the natural organic matter in the authentic water samples (TOC of WW = 10.2 mg C L^{-1}, TOC of SW = 7.8 mg C L^{-1}). Fig. 6 presents time-dependent changes in phenol (a), TOC (b) and PS (c) concentrations during NP/PS treatment of phenol in DW, SW and WW. As shown in Fig. 6a, it is apparent that phenol reduction was appreciably inhibited in the SW, WW samples as being expected due to its organic and inorganic content. Phenol removal decreased from 95% in DW to 29% in SW, while 1% of phenol removal occurred in the WW sample. The inhibition of the radical was mainly due to the organic matter, bicarbonate in water matrix, as both are usually present in the aquatic environment and act as radical scavenger via competing radicals. As shown in Fig. S7a, when 10 mg L^{-1} of NOM concentration (similar concentration with the TOC in SW = 7.8 mg L^{-1} and WW = 10.2 mg L^{-1}) was added, the phenol degradation rate decreased significantly with 20% phenol residual. It has been reported that NOM contain many phenolic hydroxyl and carboxyl groups, which can be adsorbed onto catalyst surface and block reactive sites, thus to inhibit the oxidation process [47]. Moreover, the alkalinity in SW and WW can be expressed as 11.5 mg $CaCO_3$ L^{-1} = 14 mg $NaHCO_3$ L^{-1}; 17.6 mg $CaCO_3$ L^{-1} = 20.4 mg $NaHCO_3$ L^{-1}. As shown in Fig. S7b, the removal of phenol decreased significantly and almost totally inhibited when 10 mg L^{-1} or 20 mg L^{-1} bicarbonate were added. This can be attributed to that bicarbonate could form complexes on NP surface and quench the $^{\bullet}SO_4^-$ via reactions to generate the carbonate radical ($^{\bullet}CO_3^-$) with lower activity [48].

Moreover, the TOC removals were found as 100% (0.72 mg L^{-1}), 25.9% (2.02 mg L^{-1}) and 17.5% (1.78 mg L^{-1}) in phenol spiked DW, SW and WW samples, respectively (Fig. 6b). The higher TOC abatement achieved in the treated SW and WW samples might be attributable to the higher, readily oxidisible TOC fraction in the water sample, which was selectively oxidized ahead of phenol and thus competing with phenol for ROS. Obviously, the presence of phenol in these samples did not hinder the removal of their TOC content, although the presence of TOC negatively influenced phenol degradation. These results inferred that the selectivity and reactivity of generated $^{\bullet}OH$ and $^{\bullet}SO_4^-$ play a key role in the treatment performance of NP/PS system.

PS consumptions observed during phenol removal in different water/wastewater samples were depicted in Fig. 6c. PS consumptions particularly followed the corresponding phenol removals being highest in DW (0.35 mmol L^{-1}), followed by WW (0.24 mmol L^{-1}), however deviated from the trend for SW spiked with phenol (0.18 mmol L^{-1}), where lowest PS consumption was obtained. In the SW, phenol degradation was dramatically inhibited, but at the same time the highest TOC removal was achieved, indicating that the treatment performance of both parameters affected PS consumption profiles.

3.7. Acute toxicity

Considering the substantially better performance of the NP/PS process in DW and SW samples, it was decided to perform the acute toxicity tests in these two water samples. In this study, V. fischeri was selected to monitor acute toxicity changes during NP/PS treatment of phenol-spiked DW and SW, since this test organism is widely utilized in AOPs applications [48]. Changes in acute toxicity

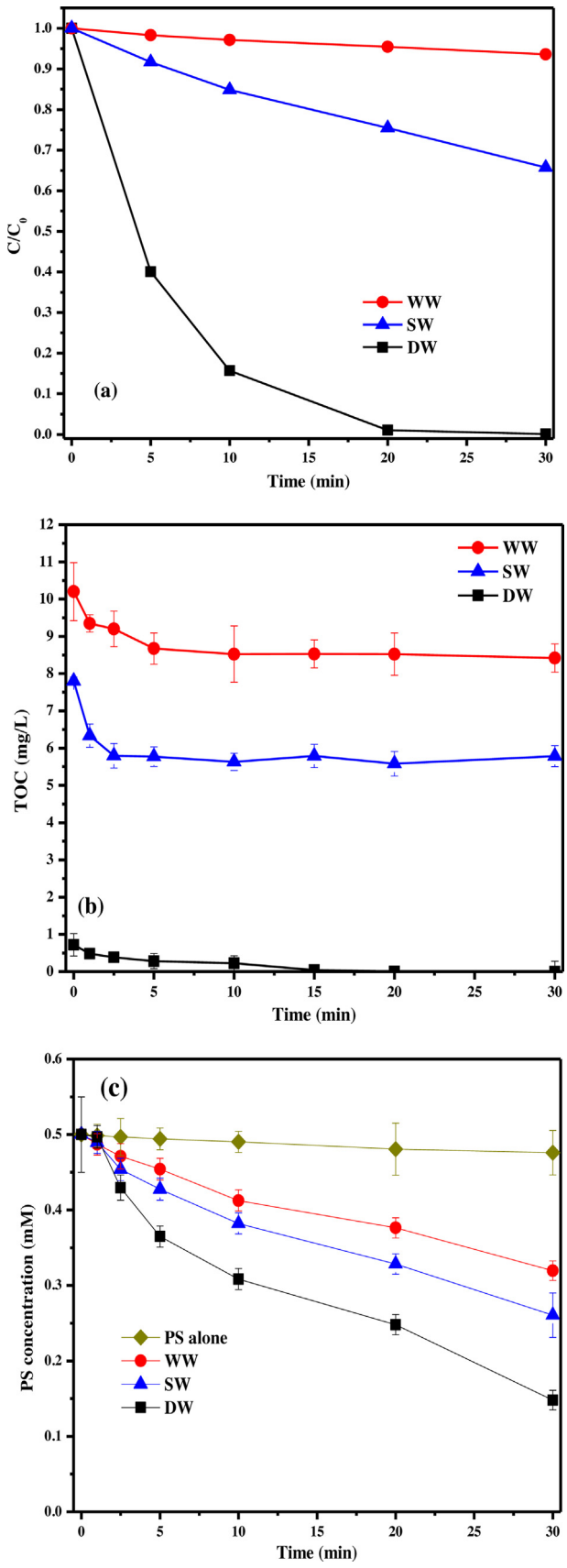

Fig. 6. Phenol (a), TOC (b) and PS (c) abatements during NP/PS treatment of phenol in DW, SW, WW. Experimental conditions: [phenol] = 20 μmol L^{-1}, [PS] = 0.5 mmol L^{-1}, [NP] = 1.25 g L^{-1}.

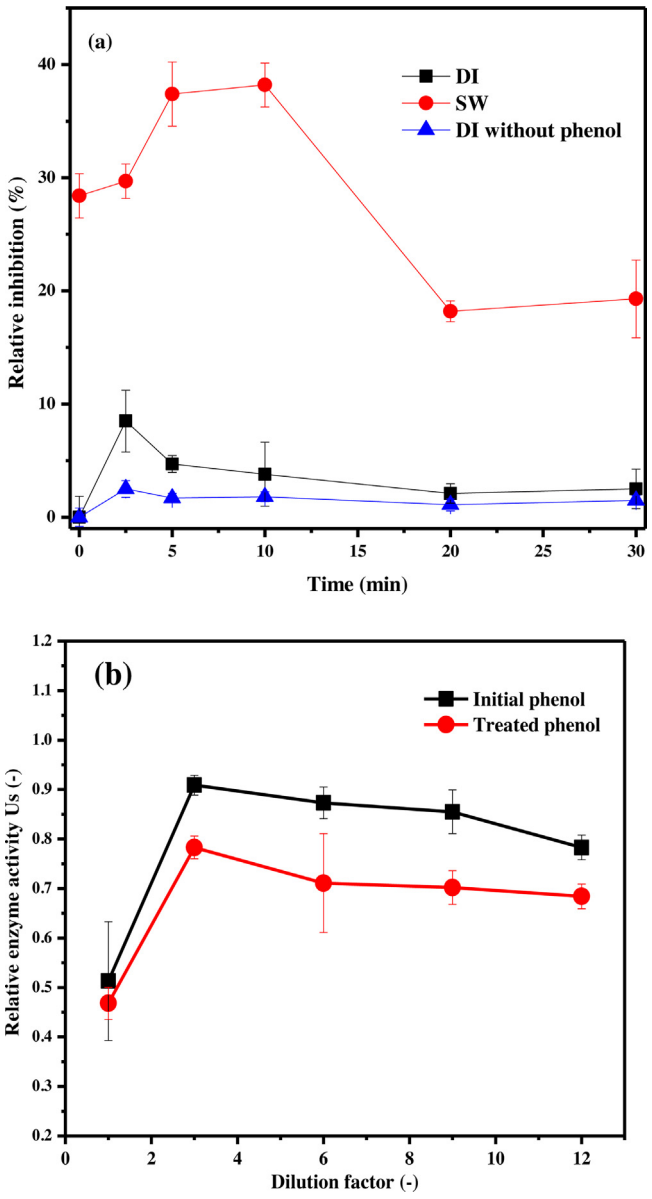

Fig. 7. (a) Changes in percent relative inhibition towards *V. fischeri* during NP/PS treatment of phenol in DW and SW, (b) Relative enzyme activities (U_S values) for the initial and 60 min-treated phenol in DW for different dilution rates (factors) in the range of 1:1.5-1:12. Experimental conditions: [phenol] = 20 μmol L^{-1}, [PS] = 0.5 mmol L^{-1}, [NP] = 1.25 g L^{-1}.

are presented in terms of% relative photoluminescence and growth inhibition rates towards V. fischeri as a function of treatment time. Fig. 7a shows the toxic response as percent relative inhibition being recorded after a 15 min incubation period. It is apparent that phenol is not a substantially toxic chemical towards the photobacterium *V. fischeri*, as the original phenol solution (measured for t = 0 min) exerted no toxic behavior in the DW (0% inhibition). However, the original phenol solution in SW sample (measured for t = 0 min) exerted more toxic behavior with 28.4% inhibition. This may suggest that some toxic substances existed in the SW water sample. Moreover, the inhibitory/toxic effect increased at the initial stages (0–2.5 min in DW; 0–10 min in SW), most probably due to accumulation of relatively toxic degradation products (aromatic fragmentation products of phenol) followed by a substantial reduction in the inhibition rates after 30 min NP/PS treatment in both water matrices. Due to the poor TOC removals obtained in SW, the inhibitory/toxic response did not totally disappear remaining at

Table 2
Induction ratios (I_R values) determined for the initial and 30 min-treated phenol in DW.

Dilution ratio	Original	Treated
1:1.5	0.62	0.81
1:3.0	0.77	0.95
1:6.0	0.87	0.71
1:12	0.83	0.91

19% in SW sample. Obviously, the acute toxicity data indicated that no toxicity increased at the end of NP/PS treatment in contrast with the initial conditions. Moreover, no significant inhibition of *V. fischeri* was observed for NP/PS solution, indicating the toxicity from residual oxidants is limited. This is reasonable, as the residual PS in the solution will quickly decompose and diminish during sampling and preparation of incubation. Therefore, compared with the result of treated phenol in DI water, it exhibited some inhibition in the initial time, further confirming the toxicity is mainly from the intermediate of phenol degradation. The bioassay results also revealed that *V. fischeri* inhibition was seriously affected by the environmental characteristics of the water samples, the efficiency/performance of the studied treatment process.

3.8. Genotoxicity

There is rarely study about the genotoxic activity during application of AOPs to treat micro-pollutants [49]. By employing the genotoxic activity test, it is possible to identify toxic chemicals due to their ability to induce mutations and cancerous transformation of normal cells [50]. Besides, the test protocol enables the calculation of the β-galactosidase activity *Us* (in relative units) after 30 min incubation as well as the *Umu induction ratio* I_R after 60 min incubation, both of which are appropriate indicators of a genotoxic response. Fig. 7b depicts the relative enzyme activities (*Us values*) for the phenol solution before and after 30 min NP/PS treatment in DW under the aforementioned reaction conditions at varying dilution rates. The *Us* values firstly increased with increasing dilution ratio (from 1:1.5 to 1:3.0), and a slight decrease was observed upon elevation of the dilution ratio from 1:3 to 1:6 and 1:12. This trend was observed for both initial phenol and treated phenol samples. Since the readings at the lowest dilution ratio (1:1.5) were lowest being recorded as 0.513 and 0.468 for the initial and treated phenol samples, respectively, and increased abruptly for the higher dilution, thereafter decreasing with increasing dilution factor, it might be deduced that both samples were cytotoxic [36]. This observation might also be supported by the I_R values summarized in Table 2 that are presenting calculations for both the initial and treated phenol samples. According to the test protocol, the I_R values must be >1.5 to consider a test sample to be genotoxic [36,51], which is not the case for the phenol samples examined in this work. Therefore, genotoxic activity tests indicated that the initial and NP/PS treated samples were not genotoxic but cytotoxic.

4. Conclusions

The NP/PS system was more effective than NP/H_2O_2 system for phenol removal. Aerobic and acidic conditions were more beneficial for phenol degradation due to more generation of $^{\bullet}SO_4^-$ and $^{\bullet}OH$. The leaked Fe^{2+} and ≡Fe(II) of NP collectively work to activate PS and generate series of surface and bulk $^{\bullet}SO_4^-$ and $^{\bullet}OH$. In addition, phenol degradation was inhibited in both SW and WW but TOC concentrations in water samples were greatly decreased. The acute toxicity tests conducted for NP/PS treatment in DW and SW, percent relative inhibition rates exhibited a fluctuating trend in both water matrixes. Genotoxic activity tests indicated that the NP/PS treated samples were not genotoxic but cytotoxic. The results of this study suggest the NP/PS process can be a promising approach for the degradation of the refractory micropollutants in the aqueous systems.

Acknowledgement

The project was supported by a research grant (GRF14100115) of the Research Grant Council, Hong Kong SAR Government and the Technology and Business Development Fund (TBF15SCI008) of The Chinese University of Hong Kong to P.K. Wong, and the research grants (41573086, 41425015 and 41603097) of National Science Foundation of China to G.Y. Li, T.C. An, D.H. Xia, respectively. P.K. Wong was also supported by CAS/SAFEA International Partnership Program for Creative Research Teams of Chinese Academy of Sciences.

Appendix A. Supplementary data

Supplementary data associated with this article can be found, in the online version, at http://dx.doi.org/10.1016/j.jhazmat.2017.07.029.

References

[1] M. Huerta-Fontela, M.T. Galceran, F. Ventura, Occurrence and removal of pharmaceuticals and hormones through drinking water treatment, Water Res. 45 (2010) 1432–1442.
[2] M.O. Barbosa, N.F.F. Moreira, A.R. Ribeiro, M.F.R. Pereira, A.M.T. Silva, Occurrence and removal of organic micropollutants: an overview of the watch list of EU Decision 2015/495, Water Res. 94 (2016) 257–279.
[3] K. Zhang, A. Randelovic, D. Page, D.T. McCarthy, A. Deletic, The validation of stormwater biofilters for micropollutant removal using in situ challenge tests, Ecolo. Eng. 67 (2014) 1–10.
[4] M.H. Al-Malack, B.O. Ahmed, Effect of presence of chemical species on removal of phenol in electrocoagulation process, Desal. Wat. Treat. 57 (2016) 11944–13994.
[5] B. Petrie, R. Barden, B. Kasprzyk-Hordern, A review on emerging contaminants in wastewaters and the environment: current knowledge, understudied areas and recommendations for future monitoring, Water Res. 72 (2015) 3–27.
[6] P. Westerhoff, Y. Yoon, S. Snyder, E. Wert, Fate of endocrine-disruptor, pharmaceutical, and personal care product chemicals during simulated drinking water treatment processes, Environ. Sci. Technol 39 (2005) 6649–6663.
[7] K.S. Sra, N.R. Thomson, J.F. Barker, Persistence of persulfate in uncontaminated aquifer materials, Environ. Sci. Technol. 44 (2010) 3098–3104.
[8] P. Sun, C. Tyree, C.H. Huang, Inactivation of Escherichia coli Bacteriophage MS2, and Bacillus spores under UV/H_2O_2 and UV/peroxydisulfate advanced disinfection conditions, Environ. Sci. Technol. 50 (2016) 4448–4458.
[9] M.G. Antoniou, A.A. de la Cruz, D.D. Dionysiou, Intermediates and reaction pathways from the degradation of microcystin-LR with sulfate radicals, Environ. Sci. Technol. 44 (2010) 7238–7244.
[10] G.P. Anipsitakis, D.D. Dionysiou, M.A. Gonzalez, Cobalt-mediated activation of peroxymonosulfate and sulfate radical attack on phenolic compounds. Implications of chloride ions, Environ. Sci. Technol. 40 (2006) 1000–1007.
[11] B. Jiang, Y. Liu, J. Zheng, M. Tan, Z. Wang, M. Wu, Synergetic transformations of multiple pollutants driven by Cr(VI)-sulfite reactions, Environ. Sci. Technol. 49 (2015) 12363–12371.
[12] X. Wang, Y. Qin, L. Zhu, H. Tang, Nitrogen-doped reduced graphene oxide as a bifunctional material for removing bisphenols: synergistic effect between adsorption and catalysis, Environ. Sci. Technol. 49 (2015) 6855–6864.
[13] R.L. Johnson, P.G. Tratnyek, R.O.B. Johnson, Persulfate persistence under thermal activation conditions, Environ. Sci. Technol. 42 (2008) 9350–9356.
[14] R.H. Waldemer, P.G. Tratnyek, R.L. Johnson, J.T. Nurmi, Oxidation of chlorinated ethenes by heat-activated persulfate: kinetics and products, Environ. Sci. Technol. 41 (2007) 1010–1015.
[15] H. Zeng, S. Liu, B. Chai, D. Cao, Y. Wang, X. Zhao, Enhanced photoelectrocatalytic decomplexation of Cu-EDTA and Cu recovery by persulfate activated by UV and cathodic reduction, Environ. Sci. Technol. 50 (2016) 6459–6466.
[16] A. Rastogi, S.R. Al-Abed, D.D. Dionysiou, Sulfate radical-based ferrous-peroxymonosulfate oxidative system for PCBs degradation in aqueous and sediment systems, Appl. Catal. B Environ. 85 (2009) 171–179.
[17] L. Zhou, W. Song, Z. Chen, G. Yin, Degradation of organic pollutants in wastewater by bicarbonate-activated hydrogen peroxide with a supported cobalt catalyst, Environ. Sci. Technol. 47 (2013) 3833–3839.
[18] P. Drzewicz, L. Perez-Estrada, A. Alpatova, J.W. Martin, M. Gamal El-Din, Impact of peroxydisulfate in the presence of zero valent iron on the oxidation

of cyclohexanoic acid and naphthenic acids from oil sands process-affected water, Environ. Sci. Technol. 46 (2012) 8984–8991.
[19] M. Usman, P. Faure, C. Ruby, K. Hanna, Application of magnetite-activated persulfate oxidation for the degradation of PAHs in contaminated soils, Chemosphere 87 (2012) 234–240.
[20] L. Zhu, Z. Ai, W.K. Ho, L. Zhang, Core–shell Fe-Fe_2O_3 nanostructures as effective persulfate activator for degradation of methyl orange, Sep. Pur. Technol. 108 (2013) 159–165.
[21] A.L.T. Pham, C. Lee, F.M. Doyle, D.L. Sedlak, A silica-supported iron oxide catalyst capable of activating hydrogen peroxide at neutral pH values, Environ. Sci. Technol. 43 (2009) 8930–8935.
[22] Y. Ren, L. Lin, J. Ma, J. Yang, J. Feng, Z. Fan, Sulfate radicals induced from peroxymonosulfate by magnetic ferrospinel MFe_2O_4 (M = Co, Cu Mn, and Zn) as heterogeneous catalysts in the water, Appl. Catal. B Environ. 165 (2015) 572–578.
[23] Y. Feng, D. Wu, Y. Deng, T. Zhang, K. Shih, Sulfate radical-mediated degradation of sulfadiazine by $CuFeO_2$ rhombohedral crystal-catalyzed peroxymonosulfate: synergistic effects and mechanisms, Environ. Sci. Technol. 50 (2016) 3119–3127.
[24] Y. Wang, H. Sun, H.M. Ang, M.O. Tadeí, S. Wang, Facile synthesis of hierarchically structured magnetic MnO_2/$ZnFe_2O_4$ hybrid materials and their performance in heterogeneous activation of peroxymonosulfate, ACS Appl. Mater Inter. 6 (2014) 19914–19923.
[25] W. Li, R. Orozco, N. Camargos, H. Liu, Mechanisms on the impacts of alkalinity, pH, and chloride on persulfate-based groundwater remediation, Environ. Sci. Technol. 51 (2017) 3948.
[26] H. Liu, T.A. Bruton, W. Li, J.V. Buren, C. Prasse, F.M. Doyle, D.L. Sedlak, Oxidation of benzene by persulfate in the presence of Fe(III)- and Mn(IV)-containing oxides: stoichiometric efficiency and transformation products, Environ. Sci. Technol. 50 (2016) 890.
[27] A.L. Teel, M. Ahmad, R.J. Watts, Persulfate activation by naturally occurring trace minerals, J. Harzad. Mater. 196 (2011) 153–159.
[28] D. Xia, Y. Li, G. Huang, C.C. Fong, T. An, G. Li, H.Y. Yip, H. Zhao, A. Lu, P.K. Wong, Visible-light-driven inactivation of Escherichia coli K-12 over thermal treated natural pyrrhotite, Appl. Catal. B Environ. 176 (2015) 749–756.
[29] D. Xia, Y. Li, G. Huang, R. Yin, T. An, G. Li, H. Zhao, A. Lu, P.K. Wong, Activation of persulfates by natural magnetic pyrrhotite for water disinfection: efficiency mechanisms, and stability, Water Res. 112 (2017) 236–247.
[30] P. Avetta, A. Pensato, M. Minella, M. Malandrino, V. Maurino, C. Minero, K. Hanna, D. Vione, Activation of persulfate by irradiated magnetite: implications for the degradation of phenol under heterogeneous photo-fenton-like conditions, Environ. Sci. Technol. 49 (2014) 1043–1050.
[31] B. Iurascu, I. Siminiceanu, D. Vione, M. Vicente, A. Gil, Phenol degradation in water through a heterogeneous photo-Fenton process catalyzed by Fe-treated laponite, Water Res. 43 (2009) 1313–1322.
[32] T. Zhang, Y. Chen, Y. Wang, J. Le Roux, Y. Yang, J.P. Croueí, Efficient peroxydisulfate activation process not relying on sulfate radical generation for water pollutant degradation, Water Res. 48 (2014) 5868–5875.
[33] H. Zhong, M.L. Brusseau, Y. Wang, N. Yan, L. Quig, G.R. Johnson, In-situ activation of persulfate by iron filings and degradation of 1, 4-dioxane, Water Res. 83 (2015) 104–111.
[34] C. Liang, C.-F. Huang, N. Mohanty, R.M. Kurakalva, A rapid spectrophotometric determination of persulfate anion in ISCO, Chemosphere 73 (2008) 1540–1543.
[35] International Organization for Standardization (ISO) 11348-3, Water Quality Determination of the Inhibitory Effect of Water Samples on the Light Emission of Vibrio Fischeri (luminescent Bacteria Test) Part 3: Method Using Freeze-dried Bacteria, International Organisation for Standardization, Geneva, 2008.
[36] UMU-Chromo TestTM, I.S.O. Kit, Version 1.2, environmental bio-Detection products, Inc. (EBPI), Ontario, 2012.
[37] D. Lin, B. Xing, Adsorption of phenolic compounds by carbon nanotubes: role of aromaticity and substitution of hydroxyl groups, Environ. Sci. Technol. 42 (19) (2008) 7254–7259.
[38] P.E. Diaz-Flores, F. López-Urı, M. Terrones, et al., Simultaneous adsorption of Cd^{2+} and phenol on modified N-doped carbon nanotubes: experimental and DFT studies, J. Colloid Interf. Sci. 334 (2) (2009) 124–131.
[39] N. Yan, F. Liu, Q. Xue, M.L. Brusseau, Y. Liu, J. Wang, Degradation of trichloroethene by siderite-catalyzed hydrogen peroxide and persulfate: investigation of reaction mechanisms and degradation products, Chem. Eng. J. 274 (2015) 61–68.
[40] G.D. Fang, D.D. Dionysiou, S.R. Al-Abed, D.M. Zhou, Superoxide radical driving the activation of persulfate by magnetite nanoparticles: implications for the degradation of PCBs, Appl. Catal. B Environ. 129 (2013) 325–332.
[41] Y. Lei, C.S. Chen, Y.J. Tu, Y.H. Huang, H. Zhang, Heterogeneous degradation of organic pollutants by persulfate activated by CuO-Fe_3O_4: mechanism, stability, and effects of pH and bicarbonate ions, Environ. Sci. Technol. 49 (2015) 6838–6845.
[42] C. Liang, Y.Y. Guo, Y.C. Chien, Y.J. Wu, Oxidative degradation of MTBE by pyrite-activated persulfate: proposed reaction pathways, Ind. Eng. Chem. Res. 49 (2010) 8858–8864.
[43] Y. Zhang, H.P. Tran, X. Du, I. Hussain, S. Huang, S. Zhou, W. Wen, Efficient pyrite activating persulfate process for degradation of p-chloroaniline in aqueous systems: a mechanistic study, Chem. Eng. J. 308 (2017) 1112–1119.
[44] X. Hou, X. Huang, F. Jia, Z. Ai, J. Zhao, L. Zhang, Hydroxylamine promoted goethite surface fenton degradation of organic pollutants, Environ. Sci. Technol. (2017), http://dx.doi.org/10.1021/acs.est.6b05906.
[45] X. Duan, H. Sun, J. Kang, Y. Wang, S. Indrawirawan, S. Wang, Insights into heterogeneous catalysis of persulfate activation on dimensional-structured nanocarbons, ACS Catal. 5 (2015) 4629–4636.
[46] X. Li, Y. Cui, Y. Feng, Z. Xie, J. Gu, Reaction pathways and mechanisms of the electrochemical degradation of phenol on different electrodes, Water Res. 39 (2005) 1972–1981.
[47] Y. Wu, A. Bianco, M. Brigante, W. Dong, P. de Sainte-Claire, K. Hanna, G. Mailhot, Sulfate radical photogeneration using Fe-EDDS: influence of critical parameters and naturally occurring scavengers, Environ. Sci. Technol. 49 (2015) 14343–14349.
[48] Y. Guan, J. Ma, Y. Ren, Y. Liu, J. Xiao, L. Lin, C. Zhang, Efficient degradation of atrazine by magnetic porous copper ferrite catalyzed peroxymonosulfate oxidation via the formation of hydroxyl and sulfate radicals, Water Res. 47 (2013) 5431–5438.
[49] S. Parvez, C. Venkataraman, S. Mukherji, A review on advantages of implementing luminescence inhibition test (Vibrio fischeri) for acute toxicity prediction of chemicals, Environ. Int. 32 (2006) 265–268.
[50] S. Frassinetti, C. Barberio, L. Caltavuturo, F. Fava, D. Di Gioia, Genotoxicity of 4-nonylphenol and nonylphenol ethoxylate mixtures by the use of Saccharomyces cerevisiae D7 mutation assay and use of this text to evaluate the efficiency of biodegradation treatments, Ecotox. Environ. Safe. 74 (2011) 253–258.
[51] A. Karci, I. Arslan-Alaton, M. Bekbolet, G. Ozhan, B. Alpertunga, H_2O_2/UV-C and Photo-fenton treatment of a nonylphenol polyethoxylate in synthetic freshwater: follow-up of degradation products, acute toxicity and genotoxicity, Chem. Eng. J. 241 (2014) 43–51.